Effect of CO_2 Nanobubble Water on the Fracture Properties of Cemented Backfill Materials under Different Aggregate Fractal Dimensions

Cao, Xiaoxiao
Department of Earth Resources Engineering, Kyushu University

Hamanaka, Akihiro
Department of Earth Resources Engineering, Kyushu University

Shimada, Hideki
Department of Earth Resources Engineering, Kyushu University

Sasaoka, Takashi
Department of Earth Resources Engineering, Kyushu University

出版情報：Applied Sciences. 14 (17), pp.7792-, 2024-09-03. Multidisciplinary Digital Publishing Institute : MDPI
バージョン：

applied sciences

MDPI

Article

Effect of CO_2 Nanobubble Water on the Fracture Properties of Cemented Backfill Materials under Different Aggregate Fractal Dimensions

Xiaoxiao Cao, Akihiro Hamanaka *, Hideki Shimada and Takashi Sasaoka

Department of Earth Resources Engineering, Kyushu University, Fukuoka 8190395, Japan; cao.xiaoxiao.037@s.kyushu-u.ac.jp (X.C.); shimada@mine.kyushu-u.ac.jp (H.S.); sasaoka@mine.kyushu-u.ac.jp (T.S.)

* Correspondence: hamanaka@mine.kyushu-u.ac.jp

Abstract: In order to cope with climate change and achieve the goal of carbon neutrality, the use of carbonization technology to enhance the performance of cement-based materials and achieve the purpose of carbon sequestration has become a very promising research direction. This paper considers the use of CO_2NBW as mixing water for cement-based materials, aiming to improve the carbonization efficiency of materials to achieve the goal of carbon neutrality. This time, the effect of CO_2NBW on cementitious filling materials under different aggregate fractal dimensions was studied through uniaxial compression tests and acoustic emission technology. The effect of CO_2NBW on the mechanical properties and crack evolution of the material was discussed. The results showed that CO_2 nanobubbles significantly improved the strength of cemented filling materials under different fractal dimensions, and the uniaxial compressive strength was most significantly improved by 23.04% when the fractal dimension was 2.7824. In addition, the characteristics of acoustic emission ring counts and energy parameters indicate that CO_2 nanobubbles help improve the overall pore structure of the sample, affecting the macroscopic strength. However, the addition of CO_2 nanobubbles reduces the limit energy storage ratio of elastic strain energy, which indicates that excessive CO_2 concentration may affect the hydration reaction of the cementing material.

Keywords: cemented backfill materials; fractal dimension; CO_2 nanobubble; energy evolution; uniaxial compression; acoustic emission

Citation: Cao, X.; Hamanaka, A.; Shimada, H.; Sasaoka, T. Effect of CO_2 Nanobubble Water on the Fracture Properties of Cemented Backfill Materials under Different Aggregate Fractal Dimensions. *Appl. Sci.* **2024**, *14*, 7792. https://doi.org/10.3390/app14177792

Academic Editor: Bin Gong

Received: 31 July 2024
Revised: 25 August 2024
Accepted: 2 September 2024
Published: 3 September 2024

1. Introduction

In the context of global response to climate change and achieving carbon neutrality goals [1,2], the mining industry faces the dual pressures of improving resource utilization efficiency [3,4] and reducing environmental impact [5]. Current mining technology is relatively mature, so in order to cope with the above pressures, research in related fields has gradually focused on carbon emission control [6], the sustainable utilization of resources [7], environmental pollution and restoration [8], etc. As an important green mining technology, mine cement-based cementing filling technology can not only effectively fill the goaf, prevent surface subsidence and geological disasters, but also utilize mine waste, reduce the construction of tailings ponds, and save land resources [9]. However, traditional mining cement-based bonding filling materials still have many shortcomings in terms of strength, durability and environmental performance, and they urgently need to be improved through technological innovation.

Cemented backfill material (CBM) is a fluid filling material formed by mixing tailings, cement and water in a certain proportion, which is then filled into the goaf of the mine through a pipeline. This technology can effectively utilize mine waste, reduce the harm of tailings accumulation to the environment, and provide a stable filling body to prevent surface subsidence and goaf collapse [10,11]. Traditional CBMs are mainly composed of

tailings, ordinary Portland cement and water. Their mechanical properties and durability depend largely on the material mix ratio and aggregate gradation [12–14]. Therefore, for this reason, many scholars have studied it from the aspects of cementing materials, aggregate gradation and admixtures. Obenaus-Emler et al. [15] conducted a systematic study on tailings as alkali-activated materials. The results showed that tailings materials have effective cementing properties. In addition, they improved the mechanical properties of tailings cementing materials through different methods (admixtures, physical grinding and high-temperature curing). Wu et al. [16] systematically evaluated the stability of cemented rockfill in filling mining strata through mechanical experiments and numerical simulations based on the optimization of aggregate grading. Zhou et al. [17] used aeolian sand-based material as the aggregate of the filling material and studied the transmission capacity and mechanical properties of the filling material by optimizing the ratio of the bonding material. Ruan et al. [18] developed a new type of cementitious material based on waste modified magnesium slag, fly ash and desulfurized gypsum. The research has been applied in field projects and meets safety requirements. The above research aims to reduce construction costs and reduce environmental pollution by selecting reasonable materials and ratios. However, CBM will inevitably produce CO_2 gas during the gelation process, which will have a significant impact on global warming [19,20]. To better move toward a low-carbon society, the recycling of construction solid waste has become a hot research direction. Among them, the use of solid waste as an aggregate for cement-based materials has been studied by a large number of scholars [21,22]. However, the bonding effect between recyclable aggregates and gel materials is significantly weaker than that between natural aggregates [23]. Therefore, relevant scholars have found that the early strength of recycled aggregates can be effectively improved by carbonization [24,25]. In addition, the strength improvement of recycled aggregate cement-based materials through ordinary carbonization is limited, and the carbonization efficiency in this process is low. So, in order to reduce this impact, this paper introduces CO_2 nanobubble water (CO_2NBW) as mixing water to provide an innovative solution for carbon sequestration. Nanobubbles are tiny bubbles with a diameter of less than 100 nanometers. They have a high specific surface area and good stability and can exist in liquid media for a long time [26]. Due to their unique gas composition, CO_2NBW can induce the formation of cement hydration products in the microscopic environment formed inside the material and improve the microstructure of the material. In addition, CO_2NBW also has a slow-release effect, which can gradually release gas during the hardening process of the material, increase the porosity of the material, and thus improve its mechanical properties and durability [27,28].

Taking the above reasons into consideration, this paper systematically discusses the uniaxial compressive strength (UCS), acoustic emission parameters and energy evolution of cemented backfill materials (CBMs) through uniaxial compression specimens and acoustic emission testing, aiming to provide new ideas and methods for the development of mine filling technology, promote the advancement of green mining technology, and promote the sustainable development of the mining industry.

2. Materials and Methods

2.1. Test Materials

The cemented backfill material is mainly composed of gel material (cement), aggregate (quartz sand) and mixing water (CO_2NBW). This study focuses on the effect of CO_2NBW on the cementitious material under different fractal dimension aggregate grading. Therefore, the selected aggregate particles are high-purity quartz sand particles, and the cement is ordinary Portland cement with a strength grade of 42.5, with densities of 2.64 g/cm^3 and 3.06 g/cm^3 respectively. The particle size distribution of cement has a significant impact on the hydration efficiency and strength of cement-based materials. Therefore, a laser particle size analyzer was used to test the cement, and the results are shown in Figure 1a. The CO_2NBW used as mixing water is generated by a micro-nano bubble machine produced by the Shanghai Zhongjing Environmental Protection Technology Co., Ltd., Shanghai, China,

model ZJC-NM-200L. Figure 1b shows the nanoparticle tracking analysis data provided by the manufacturer, and the overall size of the bubble is below 90 nm.

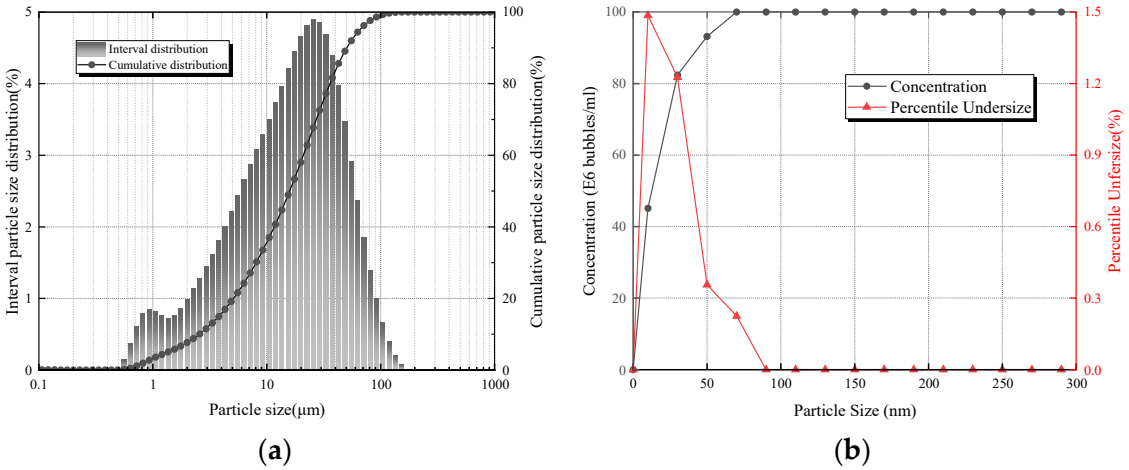

Figure 1. The distribution of particle size: cement and nanobubbles: (**a**) Cement; (**b**) nanobubble.

2.2. Test Sample Preparation

In this study, a standard cylindrical specimen (ϕ 50 mm × 100 mm) with a diameter-to-height ratio of 1:2 was selected. As the main raw material of CBM, particle size distribution is one of the important parameters of aggregate. Considering the local effect caused by particle size, the aggregate particle sizes we used were all below 8 mm, and the particle size range of aggregate particles was 7 particle size ranges, namely 1–2 mm, 2–3 mm, 3–4 mm, 4–5 mm, 5–6 mm, 6–7 mm, and 7–8 mm. Based on the fractal theory [29] shown in Equations (1) and (2), four aggregate particle size distributions with different fractal dimensions were selected, and the final calculation results are shown in Figure 2 and Table 1.

$$P_i = \frac{M_i}{M_t} = \frac{d_i^{3-D} - d_{\min}^{3-D}}{d_{\max}^{3-D} - d_{\min}^{3-D}} \quad (1)$$

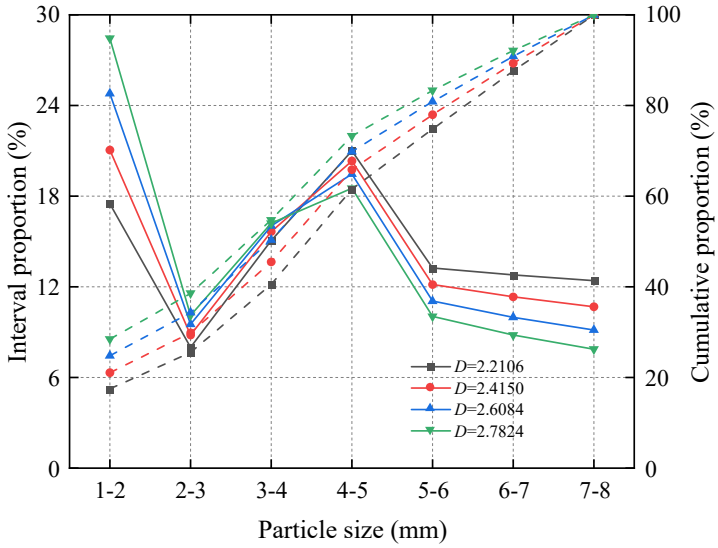

Figure 2. Aggregate particle size distribution with different fractal dimensions (Solid lines: Interval proportion; Dotted lines: cumulative proportion).

Table 1. Aggregate mass ratio in different particle size ranges.

Fractal Dimension	1–2 mm (%)	2–3 mm (%)	3–4 mm (%)	4–5 mm (%)	5–6 mm (%)	6–7 mm (%)	7–8 mm (%)
2.2106	17.49	7.99	15.06	21	13.25	12.79	12.41
2.4150	21.05	8.81	15.65	20.33	12.15	11.33	10.68
2.6084	24.79	9.53	16.03	19.47	11.05	9.98	9.14
2.7824	28.45	10.11	16.2	18.52	10.04	8.8	7.87

In the above formula, D is the fractal dimension; d_i is the pore size; d_{min} is the minimum particle size of the aggregate particles; d_{max} is the maximum particle size of the aggregate particles; M_i is the mass of the particles between d_i and d_{max}; M_t is the total mass of the particles; and P_i is the mass fraction of the particle size distribution in the particle interval.

It is worth noting that when the maximum particle size is much larger than the minimum particle size, d_{min}^{3-D} tends to 0, so the above formula can be simplified to

$$P_i = \frac{M_i}{M_t} = \left(\frac{d_i}{d_{max}}\right)^{3-D} \quad (2)$$

In this test, the gas cylinder outlet pressure was set to 0.4 MPa, the ambient temperature was about 20 °C, and the outlet pipe diameter was about 0.7 cm. Under this environmental condition, the density of CO_2 is about 1.82 kg/m^3, so according to Formula (3), the theoretical maximum flow rate of gas entering the nanobubble machine is 1320 L/min.

$$v = \sqrt{\frac{2(P_1 - P_2)}{\rho}} \quad (3)$$

In the above formula, P_1 is the cylinder pressure valve pressure, P_2 is the atmospheric pressure, and p is the CO_2 density under standard conditions.

According to Henry's law shown in Equation (4), at 20 °C and a standard atmospheric pressure, the maximum solubility of CO_2 is about 0.034 mol/L.

$$C = k_H P \quad (4)$$

In this formula, C is the solubility, k_H is the Henry constant, and P is the atmospheric pressure.

Therefore, according to the molar flow calculation formula shown in Formula (5) and the molar concentration calculation formula shown in Formula (6), the theoretical maximum intake flow rate under saturation conditions is 15.32 L/min.

$$n = \frac{Q_{CO_2}}{V_{CO_2}} \quad (5)$$

where n is the molar flow rate, Q_{CO2} is the gas flow rate, and V_{CO2} is the volume of 1 mole of CO_2 gas.

$$M = \frac{n}{Q_w} \quad (6)$$

where M is the molar concentration and Q_W is the water flow rate.

However, nanobubbles have a larger surface area and a higher gas–liquid interface ratio, which makes their contact with the liquid more complete, greatly increasing the solubility. In addition, considering the fugitive nature of the gas dissolution process, the CO_2 gas flow rate was set to 200 L/min in this test.

By adjusting the air entrainment valve of the nanobubble machine, the CO_2 entrainment rate is set to 200 L/min. After the nanobubble machine shears the CO_2 gas into nanobubbles and dissolves them in water, nanobubble water is obtained. In addition, in

this study, the water–cement ratio is set to 0.6 and the curing time is set to 28 days. The sample preparation process is shown in Figure 3, and the specific preparation scheme is shown in Table 2.

Figure 3. Sample preparation process.

Table 2. Sample preparation scheme.

Fractal Dimension	Air Inflow (L/min)	Cement (g)	Aggregate (g)	Water (mL)	Water-Cement Ratio	Curing Age (d)
2.2106	0	120	300	72	0.6	28
2.4150	0	120	300	72	0.6	28
2.6084	0	120	300	72	0.6	28
2.7824	0	120	300	72	0.6	28
2.2106	200	120	300	72	0.6	28
2.4150	200	120	300	72	0.6	28
2.6084	200	120	300	72	0.6	28
2.7824	200	120	300	72	0.6	28

3. Results

3.1. Response of Uniaxial Compressive Strength of CBM Specimens to CO_2NBW under Different Fractal Dimension Aggregate Gradations

The mechanical properties of CBM materials can be effectively evaluated by UCS. In order to analyze the effect of CO_2NBW on the compressive strength of CBM, Figure 4 shows the improvement effect of CO_2NBW on the compressive strength of the specimens under different aggregate gradings. It can be found from Figure 4a that the compressive strength of the CBM specimens shows an upward convex change trend with the fractal dimension of the aggregate. Under different mixing water conditions, UCS reaches a peak value in the range of D = 2.4150 to D = 2.6084. In addition, when CO_2NBW is added, the compressive strength of the CBM specimens is also significantly enhanced. This shows that CO_2NBW can effectively improve the hydration reaction inside the material, enhancing the strength of the specimen. In order to explore the response of CO_2NBW to different aggregate gradations, the variation law of the increase value and increase amplitude of UCS with the fractal dimension D shown in Figure 4b was obtained. It can be found that under different fractal dimensions, the sensitivity of CBM specimens to CO_2NBW is different, and the increase value and increase amplitude of UCS show a concave trend with the fractal dimension trend. When the fractal dimension is 2.4150, the minimum increase value and increase amplitude are 2.13 MPa and 10.05%, respectively. When the fractal dimension is 2.7824, the maximum increase value and increase amplitude are 4.15 MPa and 23.04%, respectively. From previous studies [30], it can be found that excellent aggregate grading usually has better density to improve material strength. The previous results show that

the improvement in strength between 2.4150 and 2.6084 is significantly better than that between 2.2106 and 2.7824, and the improvement effect of CO_2NBW on strength is more significant at 2.2106 and 2.7824. This shows that when the aggregate gradation is poor, it can be expected that the CBM material will have more pores overall, the contact area between CO_2NBW and the material will increase, and the strength increase in CO_2NBW on the CBM sample will also increase accordingly.

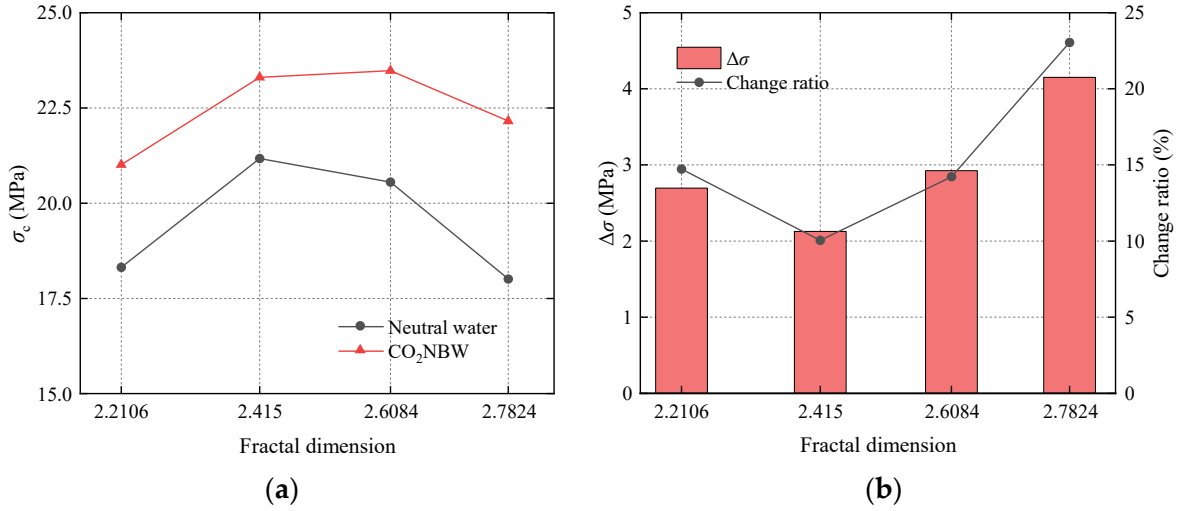

Figure 4. The variation in UCS with fractal dimension: (**a**) UCS; (**b**) UCS increase value and change ratio.

3.2. Acoustic Emission Response Mechanism of CBM Specimens

The evolution of pore cracks in materials is presented in the form of strength changes and different damage characteristics on a macro-scale. In order to explore the crack evolution mechanism, it has become a common method to detect the internal crack evolution process of materials through acoustic emission technology. Therefore, this section uses acoustic emission technology to monitor the evolution law of acoustic emission parameters of CBM specimens.

Figures 5 and 6 describe the acoustic emission counting characteristics of CBM specimens under the influence of CO_2NBW under different aggregate fractal dimensions. It is not difficult to find that the acoustic emission change characteristics under the two stages are consistent with the stress–strain curve change characteristics, which are mainly divided into five stages: pore compaction (0–a), linear elastic deformation (a–b), stable crack extension stage (b–c), unstable crack deformation (c–d), and post-peak attenuation stage (after d). Respectively, the 0–a stage represents the pore compaction phenomenon during loading, so the acoustic emission counting signal fluctuates to a certain extent in this stage [31]. As can be seen from Figures 1 and 2, the fractal dimension fluctuates significantly lower in the 0–a stage between 2.4150 and 2.6084, indicating that 2.4150 and 2.6084 are the best intervals for aggregate grading. Similarly, the addition of CO_2NBW also improves the pore structure of the CBM sample to a certain extent. In the a–b stage, the sample shows a recoverable elastic change under the action of external force, and the acoustic emission ringing change in this stage is not obvious. Point b is the crack initiation point of the sample. In the b–c stage, the internal cracks gradually increase and develop, which is reflected in the significant increase in the acoustic emission ringing count, and the stress–strain curve shows an upward convex growth trend. After point c, the crack development is uncontrollable and the stress–strain curve shows a flat trend. After point d, the stress gradually slows down after reaching the peak value, a through crack appears inside the sample, and the acoustic emission ringing count also suddenly increases to the peak value. In addition, after the ringing count reaches the peak, it still has a high value, which indicates that the CBM sample still has a certain residual strength after the peak, so the cracks continue to develop and expand in the post-peak stage.

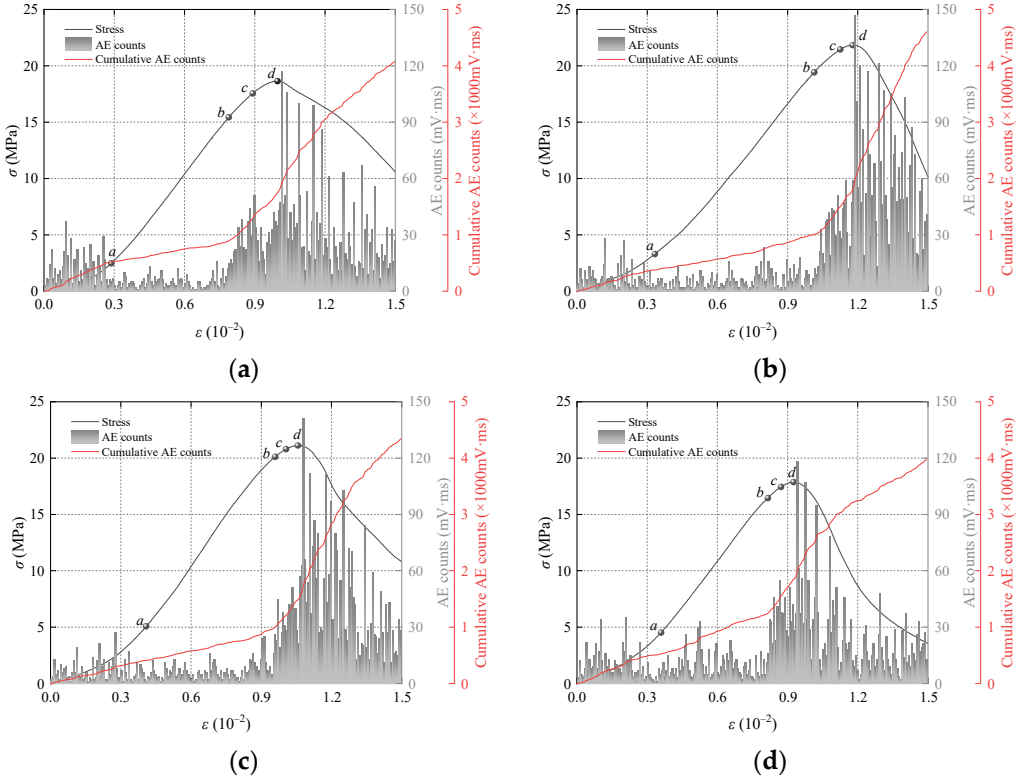

Figure 5. Variation law of acoustic emission ringing of natural water mixed CBM samples with aggregate fractal dimension: (**a**) D = 2.2106; (**b**) D = 2.4150; (**c**) D = 2.6084; (**d**) D = 2.7824.

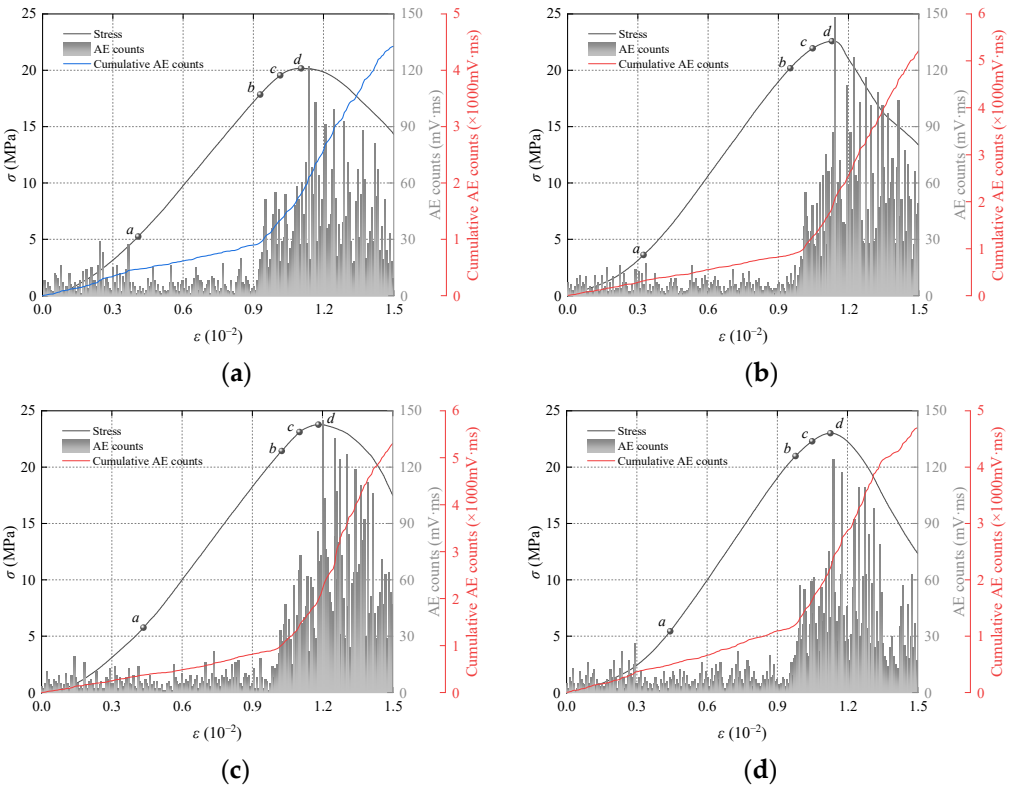

Figure 6. Variation law of acoustic emission ringing of CO_2NBW mixed CBM samples with aggregate fractal dimension: (**a**) D = 2.2106; (**b**) D = 2.4150; (**c**) D = 2.6084; (**d**) D = 2.7824.

3.3. The Changing Law of the Cumulative Acoustic Emission Counts

The cumulative ring count is closely related to the strength properties of the material. Figure 7 shows the variation in the cumulative acoustic emission ring count. The fitting shows that the cumulative acoustic emission ring count increases with the fractal dimension in an upward convex quadratic polynomial manner, and the maximum cumulative acoustic emission ring count range is between 2.4150 and 2.6084 of the fractal dimension. Moreover, the addition of CO_2NBW slightly changed the position of the peak point, and the cumulative ringing count peak point shifted from near 2.4150 to 2.6084. This phenomenon shows that the sensitivity of CBM samples with different fractal dimension aggregate gradations to CO_2NBW is different, and this result is similar to the change law of UCS.

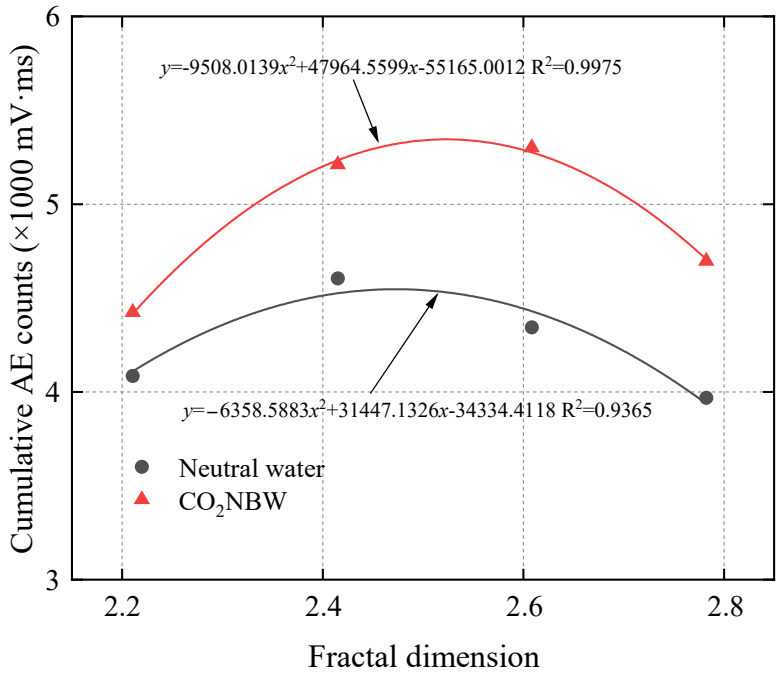

Figure 7. Variation in cumulative acoustic emission ringing counts with fractal dimension.

3.4. Energy Evolution Characteristics of CBM Specimens

In the process of material properties changing, its essential energy is also transformed. Therefore, studying the energy evolution law of CBM specimens is helpful to further explore its deformation characteristics under external forces. From the above, it is found that the CBM specimens undergo deformation processes such as dense compression, elastic deformation, plastic deformation, damage accumulation and destruction during uniaxial compression. In the above deformation process, the total energy of the external force input is converted into elastic strain energy and dissipated energy, as shown in Formula (3). The elastic strain energy is stored inside the material as a potential energy, while the dissipated energy is consumed as the material is damaged. Therefore, by exploring the changing laws of elastic strain energy and dissipated energy, the degree of damage inside the sample can be effectively characterized.

$$U = U_e + U_d, \tag{7}$$

In the above formula, U is the total input energy under the action of external force, U_e is the elastic strain energy, and U_d is the dissipated energy.

Under uniaxial compression, only the axial pressure needs to be considered, and the total input energy density of the CBM specimen can be obtained as follows:

$$U = \int_0^{\varepsilon_c} \sigma_1 d\varepsilon, \tag{8}$$

The elastic strain energy can be obtained by replacing the unloading elastic modulus with the elastic modulus of the stress–strain curve, while the dissipated energy can be obtained by substituting Equations (4) and (5) into Equation (3).

$$U_e = \frac{\sigma_1^2}{2E_u} \approx \frac{\sigma_1^2}{2E} \tag{9}$$

Through the above calculation, the energy evolution characteristics of CBM samples affected by fractal dimension under CO_2NBW mixing and conventional water mixing are obtained as shown in Figures 8 and 9. In the above study, the loading process of CBM samples can be divided into five stages. It can be seen from Figures 8 and 9 that the energy evolution curves show different change trends in the five stages. In the 0–a stage, the stress effect on the internal energy of the material is not obvious, and the dissipated energy increases most slowly. The a–b stage is the linear elastic deformation stage, and the stress–strain curve in this stage mainly shows a nearly linear growth. From the perspective of energy change, the dissipated energy maintains a low growth rate, while the total energy mainly increases significantly in the form of elastic strain energy. Stage b–c is the stage of stable crack expansion. From the above research, we know that in this stage, the cracks inside the specimen can develop in a controllable manner, which means that the proportion of dissipated energy begins to gradually increase, and the total energy curve and elastic strain energy curve change from parallel rise to divergence. In the c–d stage, cracks develop significantly, the proportion of dissipated energy increases significantly, and the elastic strain energy gradually increases to a peak value. In the destruction stage, the elastic strain energy decreases significantly until it approaches 0, and the total energy is converted to dissipated energy, and the values of the two tend to be similar.

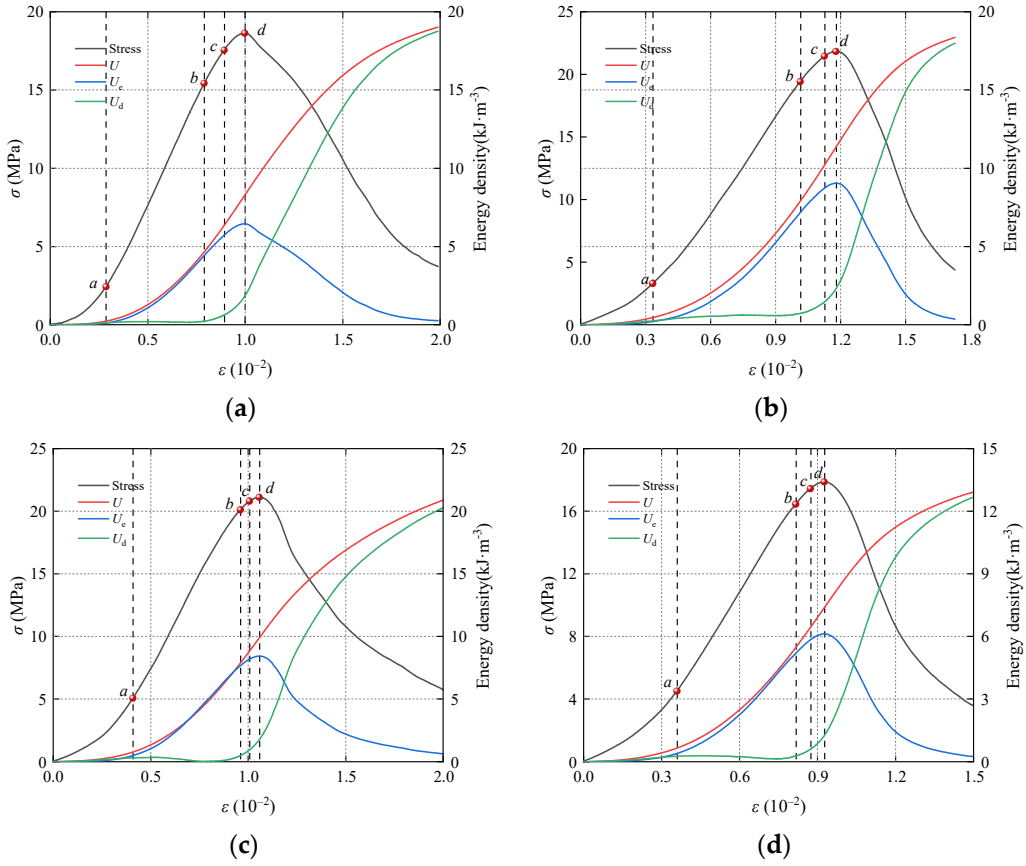

Figure 8. Variation law of energy parameters of natural water mixed CBM samples with aggregate fractal dimension: (**a**) D = 2.2106; (**b**) D = 2.4150; (**c**) D = 2.6084; (**d**) D = 2.7824.

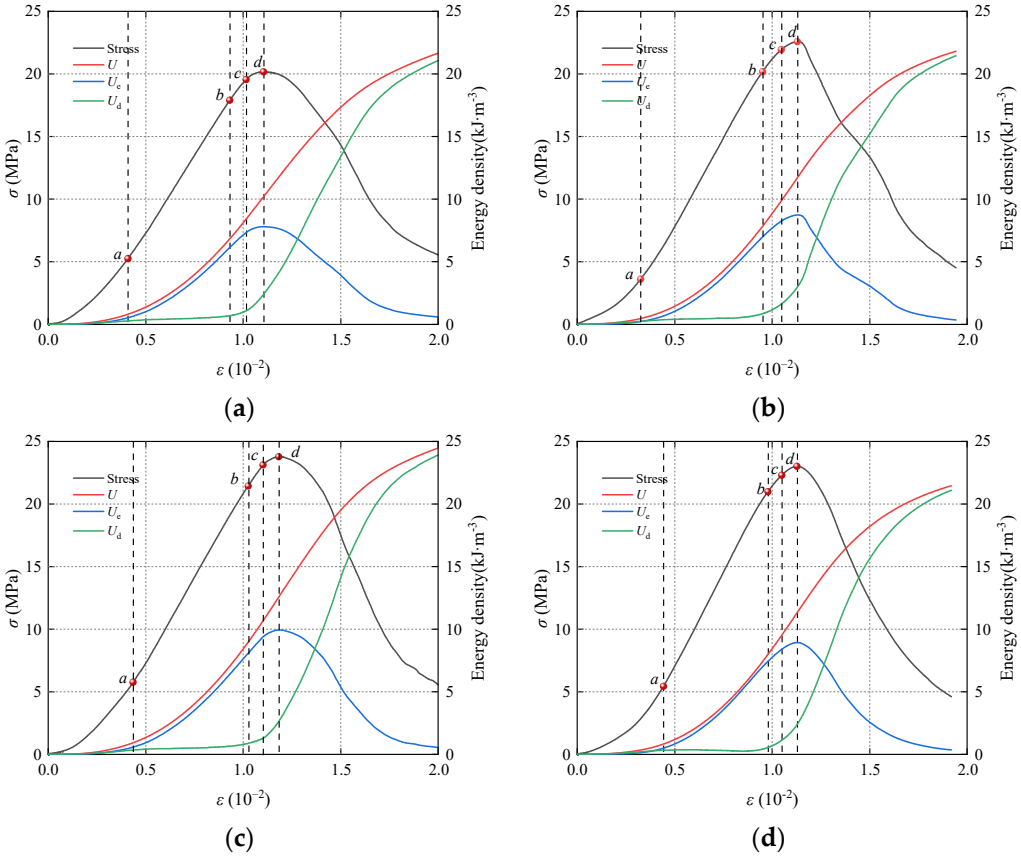

Figure 9. Variation law of energy parameters of CO_2NBW mixed CBM samples with aggregate fractal dimension: (**a**) D = 2.2106; (**b**) D = 2.4150; (**c**) D = 2.6084; (**d**) D = 2.7824.

3.5. Effects of Aggregate Fractal Dimension and CO_2NBW on Ultimate Energy Storage

In the above energy evolution process, the peak point of the stress–strain curve corresponds to the peak point of the elastic strain energy. This point reflects the maximum elastic energy storage of the material and is the limit of the energy storage. Figure 10 shows the variation in total input energy, elastic strain energy and dissipated energy at the peak stress point under the action of conventional mixing water and CO_2NBW with the fractal dimension of aggregate. It can be found that the total input energy, elastic strain energy and dissipated energy of the CBM specimens under the two mixing waters all show a trend of increasing and then decreasing. This shows that when the aggregate fractal dimension is in the range of 2.4150 to 2.6084, the energy storage capacity of the material is significantly improved, which is manifested as an increase in strength on a macro-scale. The proportion of elastic strain energy reflects the material's energy storage capacity and its ability to resist deformation during compression. Compared with conventional water mixing, the addition of CO_2NBW effectively increased various energy parameters, which further shows that the addition of CO_2NBW can effectively improve the strength performance of CBM specimens. However, through calculation, it was found that with the addition of CO_2NBW, the proportion of elastic strain energy under each fractal dimension decreased. This is inconsistent with the conclusion of the acoustic emission ring counting study that the addition of CO_2NBW can improve the pore structure of the material to a certain extent. The reason for the above results may be that CO_2NBW can effectively improve the pore structure of the material, but the CO_2 concentration design value in this study exceeds the threshold for reasonable improvement of the mechanical properties of the material, making the overly acidic environment affect the hydration process of the cement-based material. Considering the above results, the reasonable concentration threshold of CO_2 needs to be further explored in future studies.

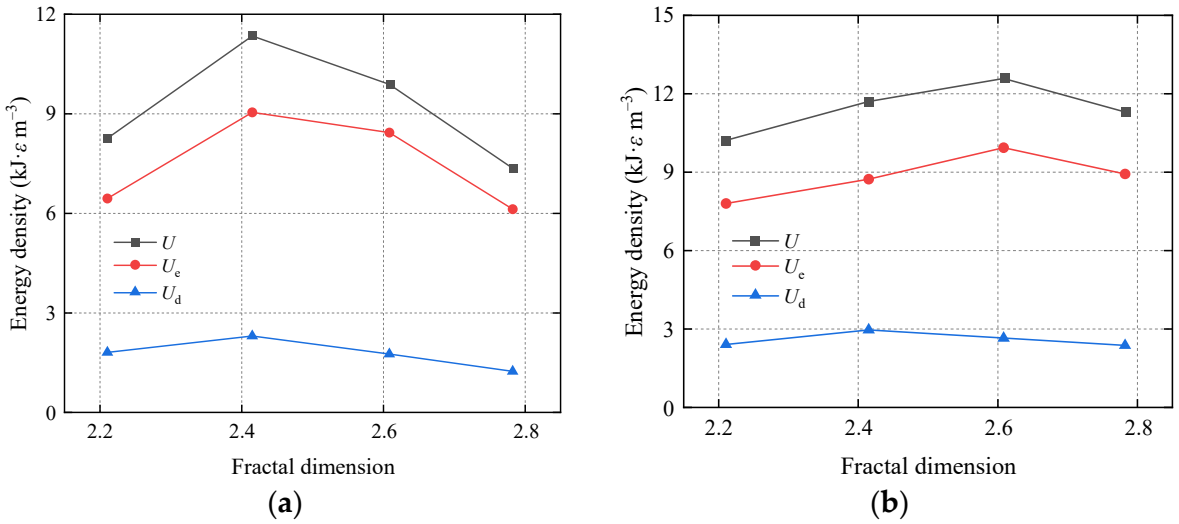

Figure 10. Relationship between energy parameters and fractal dimensions under different mixing conditions: (**a**) natural water; (**b**) CO_2NBW.

In the above energy evolution process, the peak point of the stress–strain curve corresponds to the peak point of the elastic strain energy. This point reflects the maximum elastic energy storage of the material and is the limit energy storage. Figure 10 shows the variation in total input energy, elastic strain energy and dissipated energy at the peak stress point under the action of conventional mixing water and CO_2NBW with the fractal dimension of aggregate. It can be found that the total input energy, elastic strain energy and dissipated energy of the CBM specimens under the two mixing waters all show a trend of increasing and then decreasing. This shows that when the aggregate fractal dimension is in the range of 2.4150 to 2.6084, the energy storage capacity of the material is significantly improved, which is manifested as an increase in strength on a macro-scale. The proportion of elastic strain energy reflects the material's energy storage capacity and its ability to resist deformation during compression.

3.6. Application Prospects of CO_2NBW Technology in Cement-Based Materials

In this study, there is a lack of design for the CO_2NBW concentration threshold. Considering this reason, the optimal threshold of CO_2 needs to be further explored in subsequent studies. In the conditions of this article, the design of the concentration threshold is mainly considered. From the existing research conditions, the CO_2 concentration can be determined from two aspects: direct and indirect. As the most accurate and effective means, the nanoparticle track analyzer (NTA) can effectively measure the concentration and size distribution of CO_2NBW [32]. In addition, the pH value of CO_2NBW is directly related to the CO_2 concentration [33,34]. In practical engineering applications, it is more convenient to obtain a reasonable concentration range by measuring the pH value.

In this study, CO2NBW improves the mechanics of cement-based materials from the aspects of its nanobubble characteristics and carbonation early strength characteristics. The results of this study show that after 28 days of curing, the material strength increased by 10.05% under the optimal aggregate selection. The strength increase is more significant with the deterioration of the aggregate ratio. However, some scholars have conducted relevant research on the mechanism of improving the mechanical properties of cement-based materials mainly based on a non-CO_2 solution NBW. The relevant results all show that the increase in concrete strength is in the range of 5–10% after 28 days of curing [35]. This shows that compared with other NBW, the carbonation early strength ability of CO_2NBW can further improve the mechanical properties of cement-based materials on this basis.

In addition, achieving carbon neutrality through energy conservation, emission reduction and carbon sequestration technology has become a hot topic in the current global engineering research field. Based on this background, the recycling of engineering waste (waste concrete, steel slag and fly ash, etc.) through carbonization technology can effectively improve the economic and environmental benefits of engineering industries such as construction and mining. Therefore, sustainable waste reuse through CO_2NBW has become the focus of this study's future plans.

4. Conclusions

This study focused on the influence mechanism of CO_2NBW as mixing water on the mechanical properties of cement-based materials, and it deeply explored the compressive strength, acoustic emission response and energy evolution of CBM specimens with different fractal dimension aggregate grading under the influence of CO_2NBW. The main research conclusions are as follows:

(1) The UCS of CBM specimens increases first and then decreases with the fractal dimension of aggregate gradation, and the optimal aggregate gradation range is the fractal dimension range of 2.4150 to 2.6084. In addition, CO_2NBW also significantly improves the strength of CBM specimens. However, due to the change in structural porosity caused by the change in aggregate grading, the strength improvement in the fractal dimension range of 2.4150 to 2.6084 is significantly smaller than that in the fractal dimensions of 2.2106 and 2.7824.

(2) Acoustic emission testing shows that the aggregate range of 2.4150 to 2.6084 can effectively improve the pore structure of the material. Similarly, the addition of CO_2NBW also improves the structural pores to a certain extent. In addition, the cumulative ringing count first increases and then decreases with the fractal dimension. The addition of CO_2NBW significantly increases the cumulative ringing count and causes the cumulative peak to shift to the fractal dimension of 2.6084.

(3) The energy evolution law of CBM specimens was obtained by calculating the energy evolution parameters. The results show that the energy evolution of CBM specimens can be divided into five stages, and the peak point of elastic strain energy corresponds to the peak value of the stress–strain curve. The addition of CO_2NBW and a reasonable aggregate grading interval effectively improve the values of various energy parameters. However, the addition of CO_2NBW reduces the proportion of elastic strain energy in the total energy. The reason is that excessive CO_2 concentration will affect the hydration reaction of cement-based materials, deteriorating the overall bonding effect of the specimen.

Author Contributions: Conceptualization, H.S.; writing—original draft preparation, X.C.; writing—review and editing, A.H.; validation, T.S. All authors have read and agreed to the published version of the manuscript.

Funding: Financial supports for this work was provided by China Scholarship Council (202206420019) and Obayashi Foundation (2023-research-33-57).

Institutional Review Board Statement: Not applicable.

Informed Consent Statement: Not applicable.

Data Availability Statement: The raw data supporting the conclusion of this article will be made available by the authors on request.

Acknowledgments: The authors would like to thank the editor for handling this submission and the anonymous referees for reading the manuscript. In addition, this work was also strongly supported by the China Scholarship Council and the Obayashi Foundation, to which we would like to express our gratitude.

Conflicts of Interest: The authors declare no conflicts of interest.

References

1. Murray, J.; Dey, C. The carbon neutral free for all. *Int. J. Greenh. Gas. Control.* **2009**, *3*, 237–248. [CrossRef]
2. Huovila, A.; Siikavirta, H.; Antuña Rozado, C.; Rökman, J.; Tuominen, P.; Paiho, S.; Hedman, Å.; Ylén, P. Carbon-neutral cities: Critical review of theory and practice. *J. Clean. Prod.* **2022**, *341*, 130912. [CrossRef]
3. Ju, Y.; Zhu, Y.; Xie, H.; Nie, X.; Zhang, Y.; Lu, C.; Gao, F. Fluidized mining and in-situ transformation of deep underground coal resources: A novel approach to ensuring safe, environmentally friendly, low-carbon, and clean utilisation. *Int. J. Coal Sci. Technol.* **2019**, *6*, 184–196. [CrossRef]
4. Xie, H.; Zhao, J.W.; Zhou, H.W.; Ren, S.H.; Zhang, R.X. Secondary utilizations and perspectives of mined underground space. *Tunn. Undergr. Space Technol.* **2020**, *96*, 103129. [CrossRef]
5. Song, J.; Han, C.; Li, P.; Zhang, J.; Liu, D.; Jiang, M.; Zheng, L.; Zhang, J.; Song, J. Quantitative prediction of mining subsidence and its impact on the environment. *Int. J. Min. Sci. Technol.* **2012**, *22*, 69–73. [CrossRef]
6. Ren, G.; Wang, W.; Wu, W.; Hu, Y.; Liu, Y. Carbon Emission Prediction Model for the Underground Mining Stage of Metal Mines. *Sustainability* **2023**, *15*, 12738. [CrossRef]
7. Feng, Z.; Hu, Z.; Li, G.; Zhang, Y.; Zhang, X.; Zhang, H. Improving mine reclamation efficiency for farmland sustainable use: Insights from optimizing mining scheme. *J. Clean. Prod.* **2022**, *379*, 134615. [CrossRef]
8. Rodríguez-Galán, M.; Baena-Moreno, F.M.; Vázquez, S.; Arroyo-Torralvo, F.; Vilches, L.F.; Zhang, Z. Remediation of acid mine drainage. *Environ. Chem. Lett.* **2019**, *17*, 1529–1538. [CrossRef]
9. Liu, H.; Zhang, J.; Li, B.; Zhou, N.; Xiao, X.; Li, M.; Zhu, C. Environmental behavior of construction and demolition waste as recycled aggregates for backfilling in mines: Leaching toxicity and surface subsidence studies. *J. Hazard. Mater.* **2020**, *389*, 121870. [CrossRef]
10. Li, S.; Zhang, Y.; Feng, R.; Yu, H.; Pan, J.; Bian, J. Environmental Safety Analysis of Red Mud-Based Cemented Backfill on Groundwater. *Int. J. Environ. Res. Public Health* **2021**, *18*, 8094. [CrossRef]
11. Koohestani, B.; Koubaa, A.; Belem, T.; Bussière, B.; Bouzahzah, H. Experimental investigation of mechanical and microstructural properties of cemented paste backfill containing maple-wood filler. *Constr. Build. Mater.* **2016**, *121*, 222–228. [CrossRef]
12. Wang, Y.; Wu, J.; Chen, Z. Content and gradation of aggregates effect on compaction property of gangue backfill and strata movement: Experiments and models. *Int. J. Environ. Sci. Technol.* **2022**, *19*, 10893–10910. [CrossRef]
13. Chen, W.; Zhang, G.; Tao, Q.; Yu, L.; Li, T.; Guan, X.; Guan, B. Experimental Research on Mix Ratio of Construction Waste Cemented Filling Material Based on Response Surface Methodology. *Adv. Mater. Sci. Eng.* **2022**, *2022*, 8274733. [CrossRef]
14. Li, J.; Zhang, X.; Pang, S.; Zhu, K.; Yang, C.; Zhang, X.; Su, L.; Liu, J.; Wei, X. Failure mechanism of a green substratum filling material based on digital scatter analysis. *Constr. Build. Mater.* **2024**, *418*, 135288. [CrossRef]
15. Obenaus-Emler, R.; Falah, M.; Illikainen, M. Assessment of mine tailings as precursors for alkali-activated materials for on-site applications. *Constr. Build. Mater.* **2020**, *246*, 118470. [CrossRef]
16. Wu, J.; Feng, M.; Xu, J.; Qiu, P.; Wang, Y.; Han, G. Particle Size Distribution of Cemented Rockfill Effects on Strata Stability in Filling Mining. *Minerals* **2018**, *8*, 407. [CrossRef]
17. Zhou, N.; Ma, H.; Ouyang, S.; Germain, D.; Hou, T. Influential Factors in Transportation and Mechanical Properties of Aeolian Sand-Based Cemented Filling Material. *Minerals* **2019**, *9*, 116. [CrossRef]
18. Ruan, S.; Liu, L.; Zhu, M.; Shao, C.; Xie, L. Development and field application of a modified magnesium slag-based mine filling cementitious material. *J. Clean. Prod.* **2023**, *419*, 138269. [CrossRef]
19. Kajaste, R.; Hurme, M. Cement industry greenhouse gas emissions—Management options and abatement cost. *J. Clean. Prod.* **2016**, *112*, 4041–4052. [CrossRef]
20. Teh, S.H.; Wiedmann, T.; Castel, A.; de Burgh, J. Hybrid life cycle assessment of greenhouse gas emissions from cement, concrete and geopolymer concrete in Australia. *J. Clean. Prod.* **2017**, *152*, 312–320. [CrossRef]
21. Bravo, M.; de Brito, J. Concrete made with used tyre aggregate: Durability-related performance. *J. Clean. Prod.* **2012**, *25*, 42–50. [CrossRef]
22. de Juan, M.S.; Gutiérrez, P.A. Study on the influence of attached mortar content on the properties of recycled concrete aggregate. *Constr. Build. Mater.* **2009**, *23*, 872–877. [CrossRef]
23. Talamona, D.; Hai Tan, K. Properties of recycled aggregate concrete for sustainable urban built environment. *J. Sustain. Cem. Based Mater.* **2012**, *1*, 202–210. [CrossRef]
24. Mahoutian, M.; Ghouleh, Z.; Shao, Y. Synthesis of waste-based carbonation cement. *Mater. Struct.* **2016**, *49*, 4679–4690. [CrossRef]
25. Zajac, M.; Irbe, L.; Bullerjahn, F.; Hilbig, H.; Ben Haha, M. Mechanisms of carbonation hydration hardening in Portland cements. *Cem. Concr. Res.* **2022**, *152*, 106687. [CrossRef]
26. Temesgen, T.; Bui, T.T.; Han, M.; Kim, T.I.; Park, H. Micro and nanobubble technologies as a new horizon for water-treatment techniques: A review. *Adv. Colloid. Interface Sci.* **2017**, *246*, 40–51. [CrossRef] [PubMed]
27. Kikuchi, K.; Nagata, S.; Tanaka, Y.; Saihara, Y.; Ogumi, Z. Characteristics of hydrogen nanobubbles in solutions obtained with water electrolysis. *J. Electroanal. Chem.* **2007**, *600*, 303–310. [CrossRef]
28. Wang, Z.; Bai, L.; Dong, H.; Liu, Y.; Jiang, H.; Bai, Y.; Zhang, X. Modulation of Nanobubble Behaviors through Ionic Liquids during CO_2 Electroreduction. *ACS Sustain. Chem. Eng.* **2023**, *11*, 1909–1916. [CrossRef]
29. Wang, Y.; Wu, J.; Ma, D.; Yang, S.; Yin, Q.; Feng, Y. Effect of aggregate size distribution and confining pressure on mechanical property and microstructure of cemented gangue backfill materials. *Adv. Powder Technol.* **2022**, *33*, 103686. [CrossRef]

30. Wu, J.; Wong, H.S.; Zhang, H.; Yin, Q.; Jing, H.; Ma, D. Improvement of cemented rockfill by premixing low-alkalinity activator and fly ash for recycling gangue and partially replacing cement. *Cem. Concr. Compos.* **2024**, *145*, 105345. [CrossRef]
31. Wang, B.; Yang, L.; Li, Q.; Shu, X.; Kang, M. Mechanical behavior, acoustic emission and principal strain field evolution properties of layered cemented paste backfill under unconfined compression. *Constr. Build. Mater.* **2024**, *415*, 135111. [CrossRef]
32. Feng, Y.; Han, Y.; Gao, P.; Kuang, Y.; Yang, L.; Zhao, J.; Song, Y. Study of hydrate nucleation and growth aided by micro-nanobubbles: Probing the hydrate memory effect. *Energy* **2024**, *290*, 130228. [CrossRef]
33. Antonio Cerron-Calle, G.; Luna Magdaleno, A.; Graf, J.C.; Apul, O.G.; Garcia-Segura, S. Elucidating CO(2) nanobubble interfacial reactivity and impacts on water chemistry. *J. Colloid. Interface Sci.* **2022**, *607 Pt 1*, 720–728. [CrossRef] [PubMed]
34. Liu, H.; Tian, Z.; Sun, X.; Xiang, J.; Jiao, X. Study on the multiscale properties of cement-based materials containing nano-bubble water. *Constr. Build. Mater.* **2022**, *360*, 129595. [CrossRef]
35. Chen, Y.; Han, J.-g.; Lee, J.; Shinebayar, S. Advantages of hydrogen nanobubble-rich concrete in workability and mechanical properties. *Case Stud. Constr. Mater.* **2024**, *20*, e03164. [CrossRef]